Supplementary Information:

$CoSe_2$ Necklace-like Nanowires Supported by Carbon Fiber Paper: A 3D Integrated Electrode for Hydrogen Evolution Reaction

Ke Wang[a], Dan Xi[a], Chongjian Zhou[a], Zhongqi Shi[a*], Hongyan Xia[a], Guiwu Liu[b], Guanjun Qiao[a, b*]

[a] State Key Laboratory for Mechanical Behavior of Materials, Xi'an Jiaotong University, Xi'an 710049, China

[b] School of Materials Science and Engineering, Jiangsu University, Zhenjiang 212013, China

[*] Corresponding author: zhongqishi@mail.xjtu.edu.cn (Z. Shi); gjqiao@mail.ujs.edu.cn (G. Qiao)

1 Experimental

1.1 Preparation of $CoSe_2$ necklace-like NWs on CFP

All the reagents were directly used as received. CFP was commercially available from the Toray Industries, Inc. Ultrapure water (resistivity ≈ 18.2 MΩ cm) was used throughout our experiments. The heterostructure of the electrode was synthesized through two steps, as illustrated in Fig. 1.

STEP 1: hydrothermal growth of $Co(OH)(CO_3)_{0.5}$ NWs on CFP

The method of synthesizing the $Co(OH)(CO_3)_{0.5}$ NWs was reported in our previous work[1] with a few modifications. First, the CFP was cut into 10×60 mm^2 pieces in advance. To create a clean and hydrophilic surface for the hydrothermal growth, CFP was rinsed by ethanol, H_2SO_4 solution and water in sequence ultrasonically. Then, 0.87 g $Co(NO_3)_2 \cdot 6H_2O$, 0.90 g $CO(NH_2)_2$ (Sinopharm Chemical Reagent CO., Ltd.) and 0.22 g NH_4F (Aladdin) were dissolved in 80 mL water. After the solution was transferred to a 100 mL Teflon-lined stainless steel autoclave, one piece of CFP was immersed in the solution. The autoclave was then heated in an electrical oven at 120 °C for 7 h. After cooling down to room temperature naturally, the sample was taken out and ultrasonically washed with water and ethanol. Following by drying at 80 °C, the sample was ready for the next step of selenization.

The entire hydrothermal process could be described by the following equations:[2, 3]

$$Co^{2+} + xF^- \rightarrow CoF_x^{(x-2)-}$$

$$H_2NCONH_2 + H_2O \rightarrow 2NH_3 + CO_2$$

$$CO_2 + H_2O \rightarrow CO_3^{2-} + 2H^+$$

$$NH_3 \cdot H_2O \rightarrow NH_4^+ + OH^+$$

$$CoF_x^{(x-2)-} + 0.5(2-y)CO_3^{2-} + yOH^- + nH_2O \rightarrow Co(OH)_y(CO_3)_{0.5(2-y)} \cdot nH_2O + xF^-$$

STEP 2: conversion of $Co(OH)(CO_3)_{0.5}$ NWs to necklace-like $CoSe_2$ by selenization

The sample after hydrothermal process was put into a crucible with 2 g selenium powder (Sigma-Aldrich), as shown in the inset of Fig. 1. The crucible was moved to the middle of a horizontally placed quartz tube inside a tube furnace. To investigate the process of selenization, the furnace was fast heated to different temperatures (400 to 650 °C) at a rate of 20 °C min^{-1} and held for 1 h under a steady flow of argon (99.999%) at 100 sscm. Throughout the whole heating and cooling processes, the sample was protected by the pure argon to avoid reacting with oxygen. Finally, the $CoSe_2$ NWs on CFP were completely synthesized. The loadings of $Co(OH)(CO_3)_{0.5}$ NWs on CFP were 1.40±0.2 mg cm^{-2} after the hydrothermal process and the loadings of $CoSe_2$ were 2.80, 2.70, 2.87, 2.54 and 2.48 mg cm^{-2} for selenization temperature of 450, 500, 550, 600 and 650 °C respectively.

1.2 Characterization

The crystal structure was identified by an X-ray diffractometer (XRD, PANalytical X'Pert Pro). The chemical composition was investigated by X-ray photoelectron spectroscopy (XPS) measurements using an X-ray photoelectron spectrometer (Kratos Axis Ultra DLD) with a monochromatic Al Kα irradiation source. The morphologies of $CoSe_2$ NWs on CFP were examined by scanning electron microscopy (SEM, Hitachi SU6600), high resolution transmission electron microscopy (HRTEM, JEOL JEM 2100F) and scanning transmission electron microscopy (STEM). The atomic percentage and element distribution were identified by energy dispersive spectroscopy (EDS, Oxford Instrument and EDAX Inc.). The loading of active materials was obtained with an electronic balance (0.01 mg, BT25s Sartorius).

1.3 Electrochemical evaluation

All the electrochemical measurements were performed in the 0.5 M H_2SO_4 solution using an electrochemical workstation (CHI 660D, CH Instruments, Inc.). Nitrogen gas was bubbled into electrolyte throughout the experiment. The electrochemical measurements were performed in a 3-electrode configuration. The $CoSe_2$ necklace-like NWs grown on CFP performed as the cathode for HER. A geometric electrode area of 10×10 mm^2 was defined with the help of electrochemical inert silicon rubber and directly performed as working electrode. A saturated calomel electrode (SCE) was used as the reference electrode and a graphite rod (99.9995%, Alfa Aesar) as the counter electrode. The Pt/C (20 wt% Pt on Vulcan XC-72R, Sigma-Aldrich) of the same loading with $CoSe_2$ NWs, 5 μL 5% Nafion solution (Sigma-Aldrich) and 200 μL EtOH were ultrasonically mixed and loaded on the CFP with the geometric area of 1 cm^2. The Pt/C/CFP structure was also directed used as working electrode for comparison. The reference electrode was calibrated in the hydrogen saturated electrolyte for an in situ reverse hydrogen electrode (RHE) using two Pt wires as working and counter electrodes respectively. The potential shift of the SCE was determined to be -0.266 V vs RHE. The electrocatalysis was measured using linear sweeping from 0.2 to -0.6 V (vs RHE) with a scan rate of 5 mV s^{-1}. The electrochemical impedance spectroscopy (EIS) was measured within the frequency ranging from 100 kHz to 1 Hz centering at -0.15 V (vs RHE) with an amplitude of 10 mV. The stability of electrocatalysts was examined by continuously cycling between 0.2 V and -0.3 V (vs RHE; the low potential limit was chosen to drive a current density

of approximately 30 mA cm^{-2}) at a scan rate of 200 mV s^{-1} for 5000 cycles and electrolysis at a fixed overpotential to drive the initial current density of 50 mA cm^{-2}.

1.4 Estimate of effective electrode surface area

CV is proven to be an effective method in estimating the effective electrode surface area by testing the double-layer capacitance, C_{dl}, in the non-faradaic electrochemical potential window. To determine the C_{dl}, CV was performed from 0.1 to 0.2 V (vs RHE) at the scan rates of 10, 20, 50, 100 and 200 mV s^{-1} (Fig. S7(a)). Then for each scan rate, ΔJ, the difference between anodic and cathodic current densities ($\Delta J = J_{anodic} - J_{cathodic}$) was measured at 0.15 V (vs RHE). The ΔJ was plotted against the scan rates as in Fig. S7(b). A linear fitting was conducted on the data, and C_{dl} was determined to be half the value of the fitting slope.

1.5 *iR*-correction

All the data (except for CV and EIS) presented in our manuscript have been corrected for all the ohmic losses, in order to accurately compare the performance of catalysts. The *iR*-correction is to subtract the potential loss caused by the R_s from the raw potential data, where the potential loss is calculated by the ohm's law. The R_s used in the correction could be attained form the EIS Nyquist plot as the first intercept of the main arc with the real axis. The R_s of samples synthesized at 450, 500, 550, 600 and 650 °C were 1.264, 1.350, 0.956, 1.040 and 1.900 Ω, respectively. The low and consistent R_s testify the sense of comparisons of our samples and also improve the credibility of our data. The example of *iR*-correction for the polarization curve of the sample synthesized at 450 °C is presented in Fig. S10.

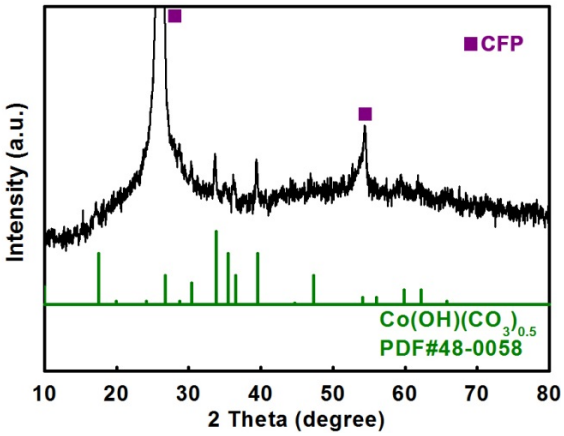

Fig. S1 XRD pattern of $Co(OH)(CO_3)_{0.5}$ NWs grown on CFP.

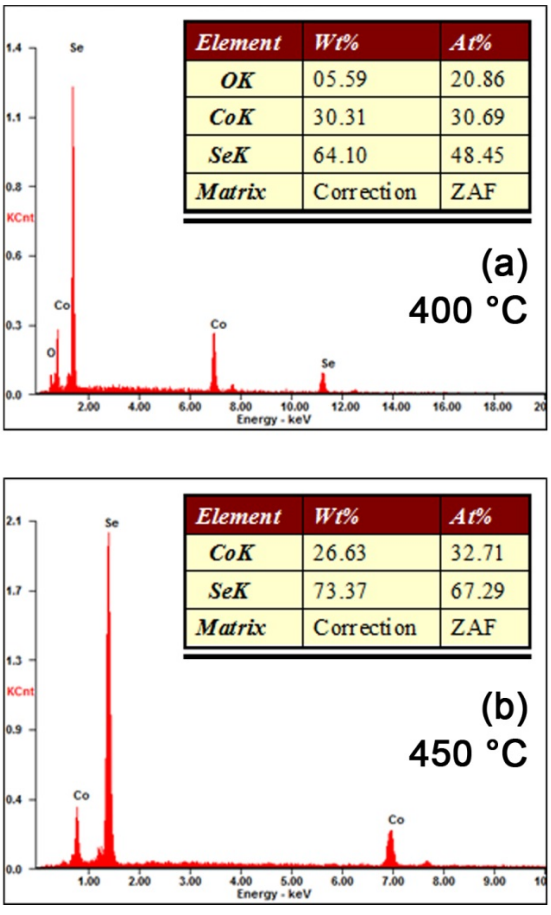

Fig. S2 The EDS spectrum of $CoSe_2$ synthesized at (a) 400 °C and (b) 450 °C

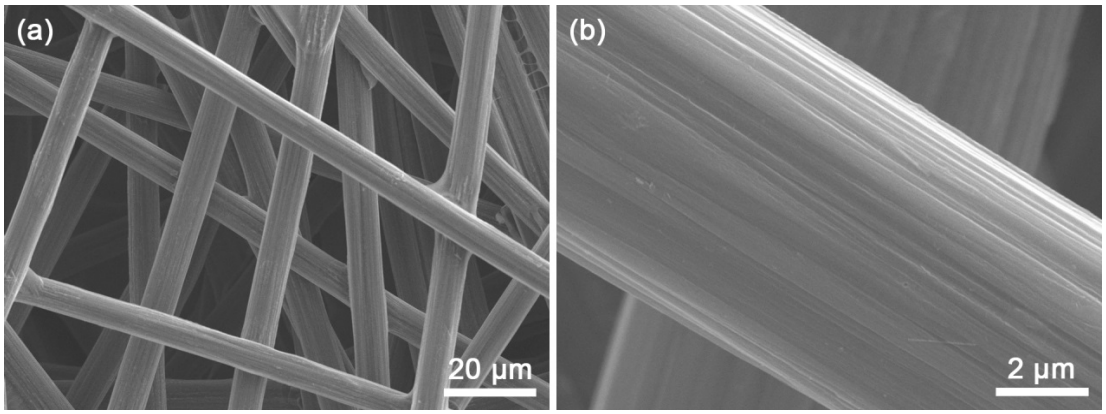

Fig. S3 (a) and (b) SEM images of bare CFP

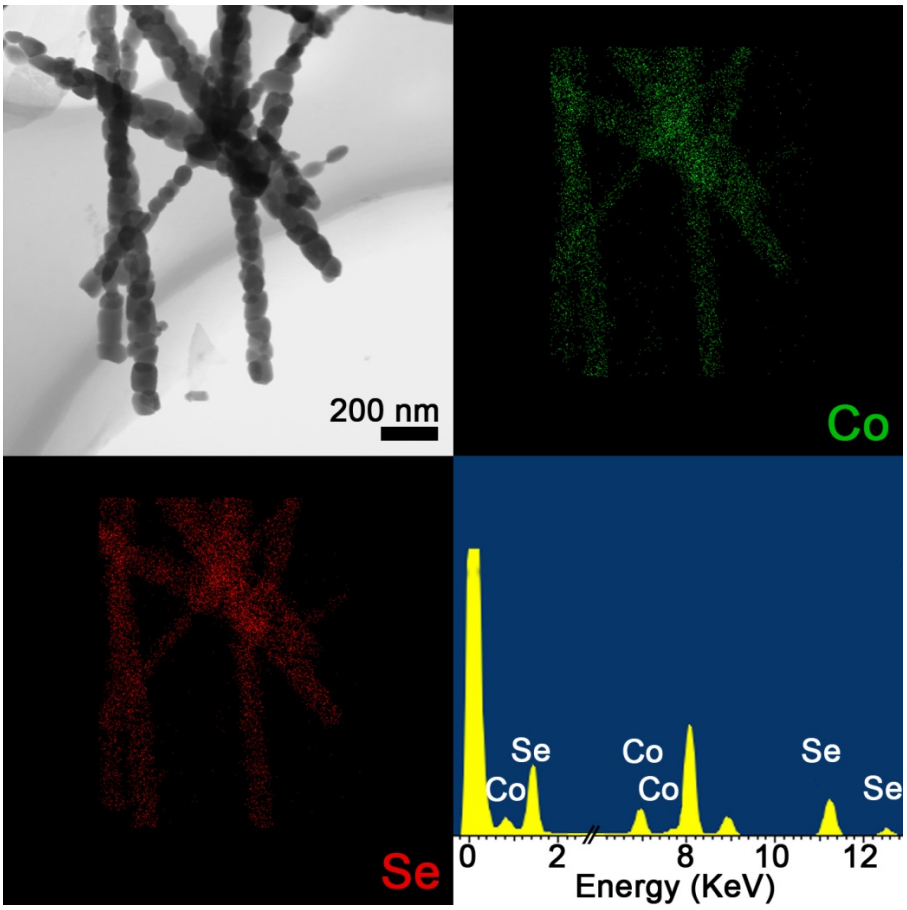

Fig. S4 STEM image of $CoSe_2$ NWs synthesized at 450 °C and the corresponding elemental mappings of Co, Se and EDS spectrum.

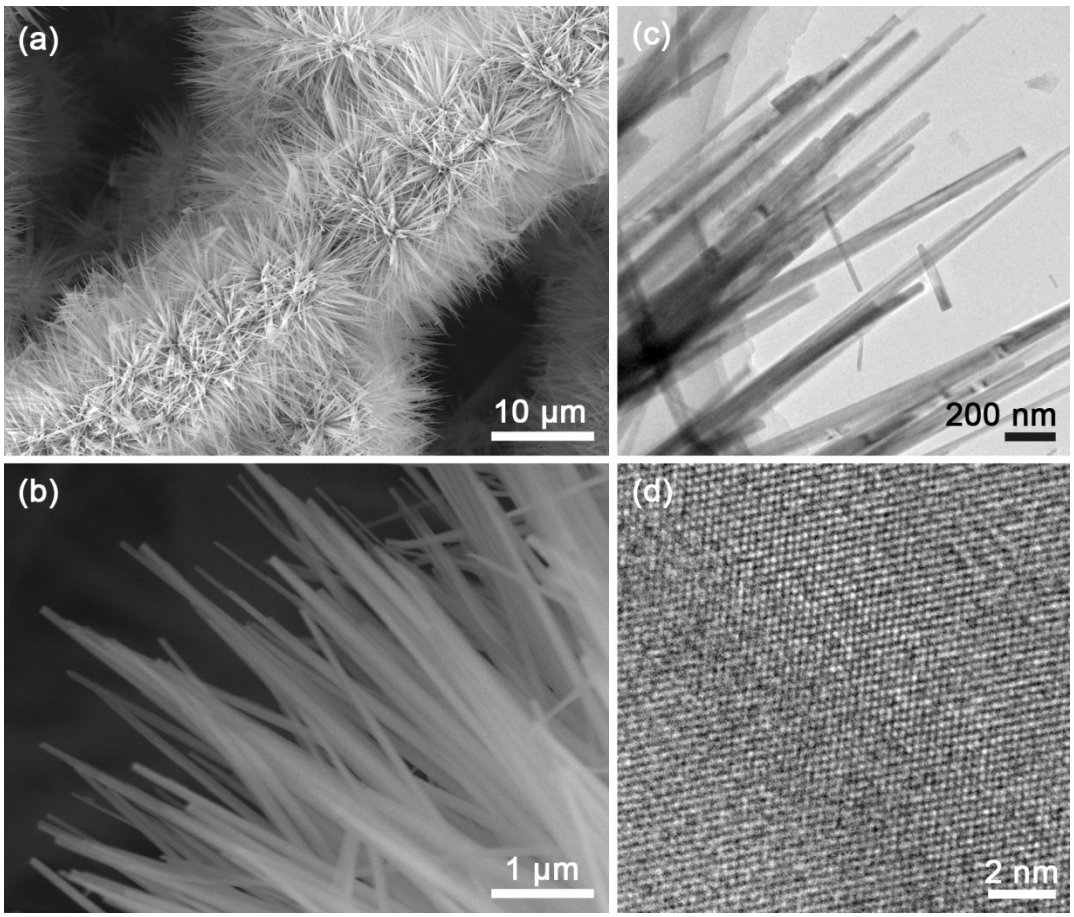

Fig. S5 (a, b) SEM and (c, d) TEM images of $Co(OH)(CO_3)_{0.5}$ NWs grown on CFP.

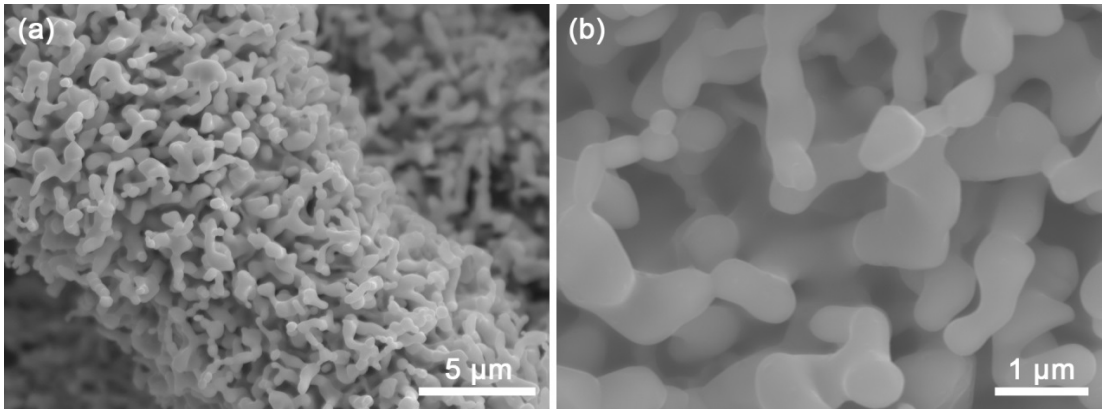

Fig. S6 (a) and (b) SEM images of $CoSe_2$ coral-like NWs synthesized at 650 °C.

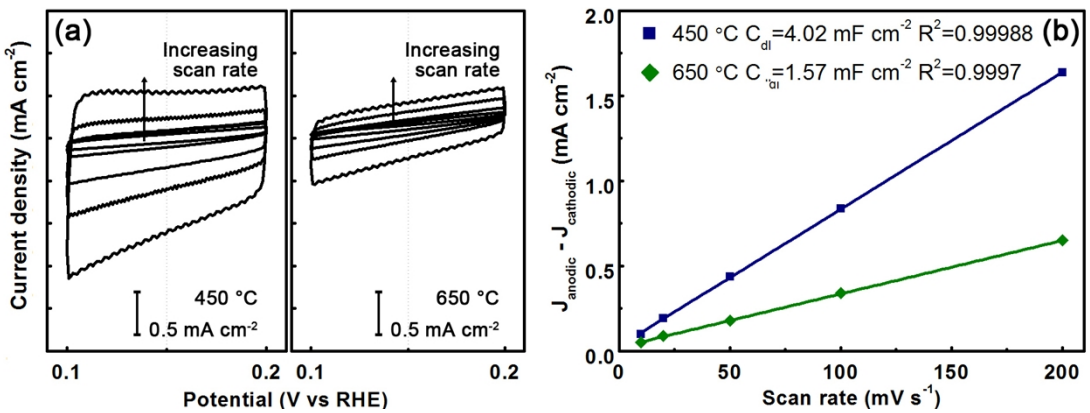

Fig. S7 (a) CV curves (10, 20, 50, 100 and 200 mV s^{-1}) of $CoSe_2$ synthesized at 450 °C and 650 °C. (b) Linear Fitting of the double-layer capacitive currents of the catalysts *vs* scan rates.

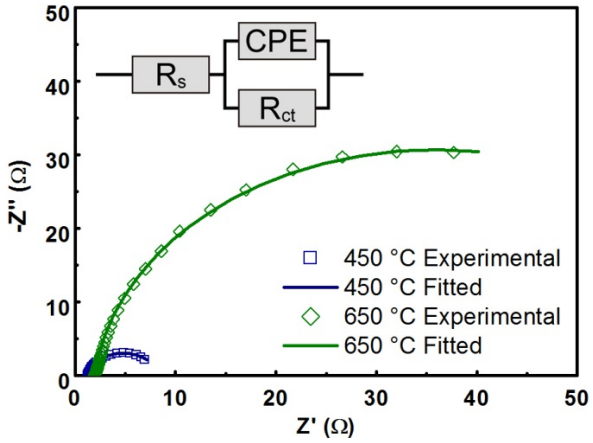

Fig. S8 Nyquist plots of $CoSe_2$ NWs on CFP at the overpotential of 150 mV. The inset shows the equivalent electrical circuit used to model the HER process.

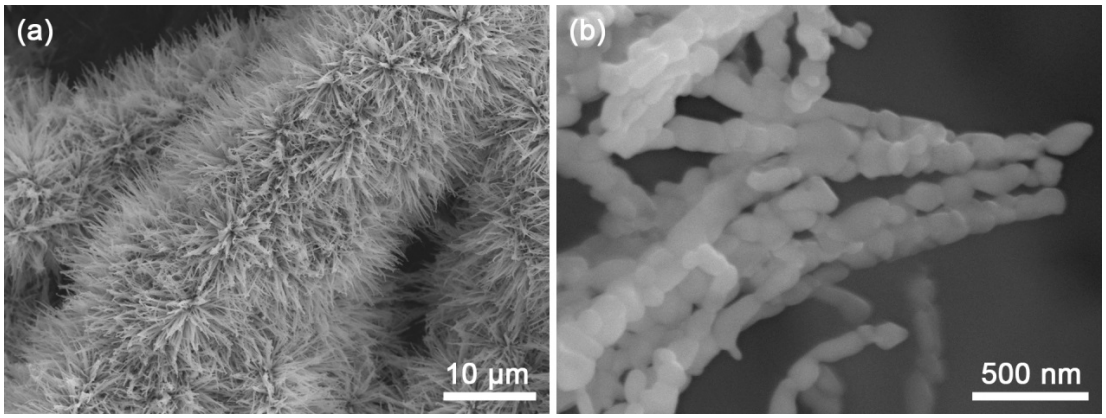

Fig. S9 (a) and (b) SEM images of $CoSe_2$ necklace-like NWs (450 °C) after the stability test.

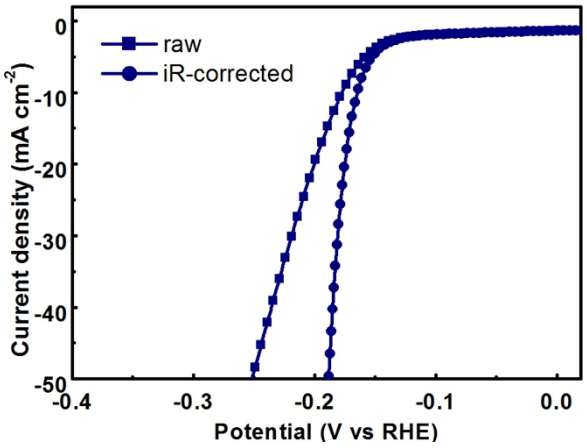

Fig. S10 Polarization curves with and without *iR*-correction of the $CoSe_2$ NWs on CFP synthesized at 450 °C.

Table S1. Comparisons of the HER performance in 0.5 M H_2SO_4 electrolyte between the $CoSe_2$ necklace-like NWs on CFP with other earth-abundant electrocatalysts.

Catalyst	Loading (mg cm^{-2})	Current density (mA cm^{-2})	Corresponding overpotential (mV)	Tafel Slope (mV dec^{-1})	Ref.
$CoSe_2$ NPs on Graphite	~2.8	10	193	42.2	4
$CoSe_2$ NPs on CFP	2.5-3.0	100	181	40	5
CoSe amorphous film	~3	100	~220	62	6
WN nanorod/CC	2.5	100	~320	92	7
WP nanorod/CC	2.0	100	~230	69	8
NiP_2 NS/CC	4.3	100	204	51	9
Ni_2P/Ni	3.5	70	~200	68	10
$NiSe_2$ NPs on CFP	2.2	100	206	50.1	5
MoS_2-Graphene/Ni	17.1	100	263	42.8	11
CoP/CC	0.92	100	~203	51	12
WS_2/CC	14	23	300	72	13
FeP/GR	4.2	50	~300	80	14
CoS_2 NWs/CP	1.7±0.3	100	~210	51.6	15
$CoSe_2$ necklace-like NWs on CFP	2.8	10; 30; 50; 100; 200	165; 181; 188; 199; 213	34.0	This work

References

1. K. Wang, Z. Shi, Y. Wang, Z. Ye, H. Xia, G. Liu and G. Qiao, *J. Alloys Compd.*, 2015, **624**, 85-93.
2. J. Jiang, J. P. Liu, X. T. Huang, Y. Y. Li, R. M. Ding, X. X. Ji, Y. Y. Hu, Q. B. Chi and Z. H. Zhu, *Cryst. Growth Des.*, 2010, **10**, 70-75.
3. X.-h. Xia, J.-p. Tu, Y.-q. Zhang, Y.-j. Mai, X.-l. Wang, C.-d. Gu and X.-b. Zhao, *RSC Adv.*, 2012, **2**, 1835.
4. H. Zhang, L. Lei and X. Zhang, *RSC Adv.*, 2014, **4**, 54344-54348.
5. D. Kong, H. Wang, Z. Lu and Y. Cui, *J. Am. Chem. Soc.*, 2014, **136**, 4897-4900.
6. A. I. Carim, F. H. Saadi, M. P. Soriaga and N. S. Lewis, *J. Mater. Chem. A*, 2014, **2**, 13835.
7. J. Shi, Z. Pu, Q. Liu, A. M. Asiri, J. Hu and X. Sun, *Electrochim. Acta*, 2015, **154**, 345-351.
8. Z. Pu, Q. Liu, A. M. Asiri and X. Sun, *ACS Appl. Mater. Inter.*, 2014, **6**, 21874-21879.
9. P. Jiang, Q. Liu and X. Sun, *Nanoscale*, 2014, **6**, 13440-13445.
10. Y. Shi, Y. Xu, S. Zhuo, J. Zhang and B. Zhang, *ACS Appl. Mater. Inter.*, 2015, **7**, 2376-2384.
11. Y. H. Chang, C. T. Lin, T. Y. Chen, C. L. Hsu, Y. H. Lee, W. Zhang, K. H. Wei and L. J. Li, *Adv Mater*, 2013, **25**, 756-760.
12. J. Tian, Q. Liu, A. M. Asiri and X. Sun, *J. Am. Chem. Soc.*, 2014, **136**, 7587-7590.
13. T.-Y. Chen, Y.-H. Chang, C.-L. Hsu, K.-H. Wei, C.-Y. Chiang and L.-J. Li, *Int. J. Hydrogen Energy*, 2013, **38**, 12302-12309.
14. J. Tian, Q. Liu, Y. Liang, Z. Xing, A. M. Asiri and X. Sun, *ACS Appl. Mater. Inter.*, 2014, **6**, 20579-20584.
15. M. S. Faber, R. Dziedzic, M. A. Lukowski, N. S. Kaiser, Q. Ding and S. Jin, *J. Am. Chem. Soc.*, 2014, **136**, 10053-10061.